





Article

PM10 Organic Aerosol Fingerprints by Using Liquid Chromatography Orbitrap Mass Spectrometry: Urban vs. Suburban in an Eastern Mediterranean Medium-Sized Coastal City

Evangelos Stergiou^{1,2,*}, Anastasia Chrysovalantou Chatziioannou^{1,3}, Spiros A. Pergantis¹
and Maria Kanakidou^{1,2,4,*}

- ¹ Environmental Chemical Processes Laboratory (ECPL), Department of Chemistry, University of Crete, Voutes Campus, 70013 Heraklion, Greece; chatziioannouc@iarc.who.int (A.C.C.); spergantis@uoc.gr (S.A.P.)
 - ² Center of Studies on Air quality and Climate Change (C-STACC), Institute of Chemical Engineering (ICE-HT), Foundation for Research and Technology (FORTH), 26504 Patras, Greece
 - ³ Nutrition and Metabolism Branch, International Agency for Research on Cancer (IARC/WHO), 69366 Lyon, France
 - ⁴ Laboratory for Modeling and Observation of the Earth System (LAMOS), Institute of Environmental Physics, University of Bremen, 28359 Bremen, Germany
- * Correspondence: stergiouvaggelis98@gmail.com (E.S.); mariak@uoc.gr (M.K.)

Abstract: This study compares the PM10 (particulate matter of diameter smaller than 10 μm) organic aerosol composition between urban and suburban stations in Heraklion, Crete, during winter 2024 in order to highlight the impact of local anthropogenic activities on urban atmospheric particulate matter pollution. Using an HPLC-ESI-MS Orbitrap analyzer (High Performance Liquid Chromatography-Electrospray Ionization-Mass Spectrometry) in full MS scan mode at a resolution of 140,000, 48 daily aerosol filter extracts were analyzed in both positive and negative modes, resulting in the detection of 2809 and 3823 features, respectively. Features with at least five times higher intensity in the urban environment compared to the suburban, and $p < 0.05$, were deemed significant. A correlation with black carbon ($r > 0.6$) was observed for 71% of significant urban features in positive mode. These features showed a predominance of low O:C ratios (< 0.2) and the majority were classified as intermediate volatility organic compounds (IVOCs), indicating fresh primary emissions. A clear urban–suburban distinction was shown by PCA of positive mode features, unlike the negative mode features. Regarding the total intensity of the features, urban samples were on average 55% higher than suburban samples in positive mode and 39% higher in negative mode. This study reveals the molecular profile of locally emitted combustion related organics observed in positive mode in an urban environment.

Keywords: PM10; urban aerosol; anthropogenic emissions; high resolution mass spectrometry; electrospray ionization; HPLC; non-target analysis; black carbon; volatility classification; combustion-related organic compounds



Citation: Stergiou, E.; Chatziioannou, A.C.; Pergantis, S.A.; Kanakidou, M. PM10 Organic Aerosol Fingerprints by Using Liquid Chromatography Orbitrap Mass Spectrometry: Urban vs. Suburban in an Eastern Mediterranean Medium-Sized Coastal City. *Air* **2024**, *2*, 311–324. <https://doi.org/10.3390/air2030018>

Academic Editor: Ling Tim Wong

Received: 31 July 2024

Revised: 28 August 2024

Accepted: 30 August 2024

Published: 3 September 2024



Copyright: © 2024 by the authors. Licensee MDPI, Basel, Switzerland. This article is an open access article distributed under the terms and conditions of the Creative Commons Attribution (CC BY) license (<https://creativecommons.org/licenses/by/4.0/>).

1. Introduction

Urban atmospheric particulate matter (PM) pollution poses significant environmental and health problems [1]. The knowledge of the pollution sources and their contribution to air quality can lead to more effective future mitigation strategies for reducing air pollution [2]. Organic aerosol (OA) is a major complex mixture of components of atmospheric PM playing an important role in air quality and climate [3–5]. Organic aerosols can originate from both primary emissions and secondary formation, with their composition and volatility influencing their atmospheric behavior and effects [6,7]. OA is an important component (20–90%) of fine PM [8]. In the regional background atmosphere, more than 60% of OA has been found to be in the submicron aerosol mode [9]. In urban areas the submicron

OA fraction can be even larger and originates from anthropogenic sources (e.g., fossil fuels, biomass burning, and cooking), as well as from secondary sources, such as chemical processing of precursor molecules in the atmosphere [8,10]. Secondary OA has been found to account for about 83.5% of OA in PM₁₀ and 86% of OA in the PM_{1.06} (PM less than 1.06 μm in diameter) in the remote Mediterranean atmosphere affected by long-range transport [11]. Stavroulas et al. [12] found that, in Athens, secondary OA accounts for 67% of sub-micron OA in winter and for more than 80% in summer. In urban environments, the high density of anthropogenic activities results in elevated concentrations of OA, particularly during periods of increased residential heating emissions [13]. These emissions contribute to the formation of primary organic aerosol (POA) and secondary organic aerosol (SOA), which results from the atmospheric oxidation of volatile organic compounds (VOC) to less volatile organics, as well as atmospheric aging of POA. The composition of OA also depends on the origin of the air masses, and therefore on distant sources of pollution that reach the study site via long-range transport, while meteorology also affects the chemical processing in the atmosphere and therefore SOA composition [14]. To model the complex mixture of OA in the atmosphere, numerical models are now commonly classifying OA components based on their volatility using the so-called Volatility Basis Set (VBS) that was first introduced in global models by Robinson et al. [15] and which classifies organics based on their volatility. Both POA and SOA have distinct molecular signatures [16,17] that also reflect in their volatility [8]. In this respect, several individual organic molecules have been reported in the literature as tracers of specific sources of PM (e.g., specific saccharides [18–20], ratios of various polyaromatic hydrocarbons [21], lipid biomarkers such as long chain n-alkanes, n-alkanols, di- and tri-unsaturated C₃₇ and C₃₈ methyl ketones and C₃₈ ethyl ketones, diols and keto-ols and a range of sterols [22], tetrols, and pinonic and pinic acids [23,24]). In the last two decades, efforts have been made to characterize the submicron fraction of OA, benefiting from the technologies developed by Aerosol Mass Spectrometer (AMS) and Aerosol Chemical Speciation Monitor (ACSM) technologies [12,25] which detect OA component families and allow near-real-time source attribution [10].

Complementary to the above techniques, high-resolution mass spectrometry (HRMS) combined with HPLC separations can be used. HPLC-ESI-MS Orbitrap is a powerful analytical technique allowing the characterization of complex organic mixtures in atmospheric aerosols [26]. HRMS provides high mass accuracy and low limits of detection enabling the identification of thousands of organic compounds [27]. This capability is particularly advantageous for non-target analysis, where comprehensive profiling of aerosol samples can reveal a wide array of compounds without prior knowledge of their identities [28].

Non-target analysis using HRMS is an unbiased method, which is essential for understanding the molecular fingerprint of organic compounds in aerosols. This approach also allows for the detection of novel compounds, providing insights into the sources and transformation processes of organic aerosols [29]. Previous studies have demonstrated the effectiveness of HRMS at identifying specific molecular tracers for different pollution sources, such as traffic emissions, biomass burning, and industrial activities [30].

The present study aims to identify differences in the organic composition between urban and suburban environments in order to highlight the impact of local anthropogenic activities on urban atmospheric PM pollution in a medium-sized coastal city. This is achieved by comparing the PM₁₀ organic aerosol composition between urban and suburban stations in Heraklion, Crete, during winter 2024. Crete, Greece, was chosen because it is located in a climate hot spot region, the East Mediterranean [31,32], and is an island far from the main continent and subject to long-range transport of air masses from the surrounding areas [33]. Depending on the trajectories of air masses reaching Crete, the area may be affected by long-range transport of Sahara dust from the south, aerosols from the Western Mediterranean Sea from the west, from Central Europe and the Balkans from the northwest and north, from the Black Sea and its surrounding countries from the northeast and from the Middle East from the east [33,34]. Therefore, the urban air quality will reflect the regional background derived from long-range transport loaded by the peri-urban

emissions and the local/urban emissions. Heraklion is therefore an ideal location to study the fingerprints of urban anthropogenic emissions. The HPLC-ESI-MS Orbitrap was used here for non-target analysis to provide detailed molecular wintertime fingerprints of the organic aerosol components in an urban and a suburban site of Heraklion.

2. Materials and Methods

2.1. Sampling Sites

Aerosol samples were collected at an urban and a suburban site of Heraklion, Crete, Greece. The urban station is located in a very small park in the city center, while the suburban station is located at 5.9 km southwest (SW) of the urban station on the campus of the University of Crete, next to the Department of Chemistry (Figure 1). The urban station is a traffic station located close to one of the city's main avenues leading to the city center and the port of Heraklion. The suburban site is a sparsely populated area with agricultural activity, mainly olive trees, where the influence of direct local anthropogenic emissions is limited. During the study period, the average temperature recorded at the urban station was $12.7\text{ }^{\circ}\text{C} \pm 1.6\text{ }^{\circ}\text{C}$, compared to $11.7\text{ }^{\circ}\text{C} \pm 1.5\text{ }^{\circ}\text{C}$ at the suburban station. The relative humidity was $61.7\% \pm 6.5\%$ at the urban station and $67.8\% \pm 5.8\%$ at the suburban station. The wind directions for both stations are classified as predominantly northwest (NW) and southeast (SE), indicating similar influences from long-range transport pollutants. The urban station shows a clearer wind direction dominance and stronger prevailing winds coming from the NW than the suburban station, which experiences stronger winds from the SW and shows a more dispersed in the wind direction pattern. Overall, the suburban station is susceptible to higher wind speeds than the urban station, with average wind speeds 2.3 m/s and 0.9 m/s, respectively. It should be noted that the wind speed at the urban station is influenced and obstructed by the taller buildings in the area, whereas the suburban station is free from direct obstruction due to its elevated location. Based on the relative locations of the stations and the prevailing winds, it is expected that there was little transport of urban emissions to the suburban station during the period studied. An analysis of the 5-day back trajectories reaching Heraklion that was carried out with the HYSPLIT model [35] showed that the extended Heraklion area was affected by transported air masses from W-SW from 7 to 13 February, then from the N-NE sector from 14 to 21 February, before becoming well mixed, regionally influenced air masses from the SW, S, and E. Overall, from 14 February to 2 March, the air masses reaching Heraklion were largely influenced by the regional sources in the eastern Mediterranean, resulting in an aged background atmospheric composition over the area studied.

2.2. Sample Collection

Aerosol sampling was performed at these two stations during wintertime, from 7 February to 2 March 2024. From each station, 24 daily filter samples were collected, totaling 48 samples. In addition, 2 field blanks were sampled. Sampling did not take place on 8 February.

A low-volume sampler (Digital DPA-14 LVS, Digital Elektronik AG, Hegnau, Switzerland) was used at each site to collect PM₁₀ particles on 47 mm diameter quartz fiber filters (PALLFLEX Membrane Filters, Tissuquartz, Pall Corporation, Port Washington, NY, USA). Sampling was performed at a flow rate of approximately 38 L min^{-1} over 24-h intervals (from 00:01 to 00:01 the day after, UTC time), corresponding to a total volume of 55 m^3 for each sample. The PM₁₀ mass was determined gravimetrically (pre- and post-weighted), using an analytical balance with 5 decimal points' precision (Kern, ABT 120-5DM, Kern & Sohn GmbH, Balingen, Germany). The filter samples were stored at $-18\text{ }^{\circ}\text{C}$ until analysis.

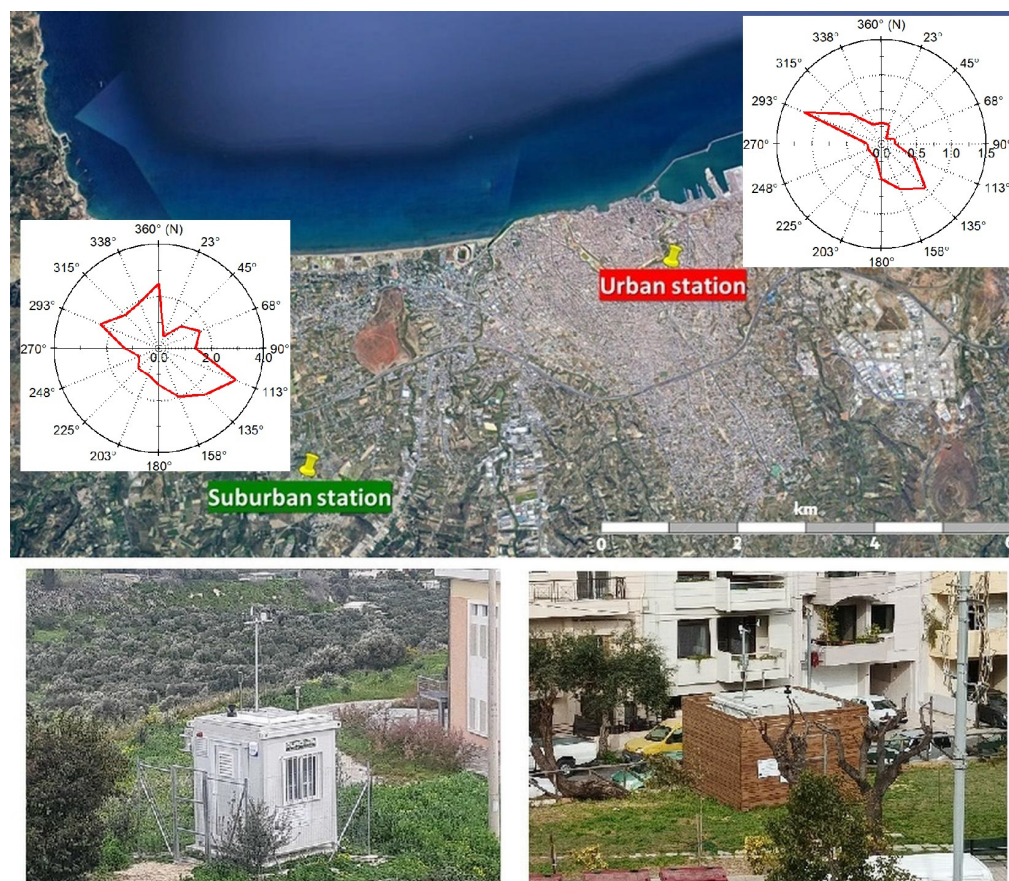


Figure 1. Satellite view of Heraklion, Crete, Greece. Urban station (right) (35.332820 N, 25.138231 E, 45 m altitude). Suburban station (left) (35.308542 N, 25.080084 E, 95 m altitude). The distance between the 2 stations is 5.9 km. The wind roses are drawn based on local winds registered at each station, averaged for the period studied. Sixteen wind direction classes are considered, wind speed units are in m/s and wind calm corresponds to 0.1 m/s.

2.3. Sample Analysis

For the analysis of the PM₁₀ aerosol samples, a punch of 1.5 cm² was cut from each quartz filter and placed inside an Eppendorf tube. For the extraction, 1 mL of acetonitrile (ACN, LiChrosolv, gradient grade for LC-MS) per sample was used. Pulsed vortexing was applied initially to each sample to ensure thorough mixing of the solvent with the sample matrix. After 1 h of extraction at room temperature with no further agitation, the extract was filtered using a 0.22 μm pore polytetrafluoroethylene (PTFE) 13 mm diameter syringe filter. The solvent was then evaporated under low pressure, and the extract was redissolved with 50 μL of 1:1 ACN/H₂O and the assistance of sonication. The dissolved samples were transferred to 2 mL glass vials with 6 mm × 31 mm glass inserts with a conical base. The sample vials were placed in the autosampler of the HPLC-MS system (Thermo Scientific UltiMate 3000 HPLC coupled with Q Exactive Plus Orbitrap, Waltham, MA, USA), conditioned at 17 °C. The two field blank filters were processed and analyzed following the same procedures as the samples. The samples were initially analyzed in positive ion mode and their re-analysis in negative ion mode followed immediately after. In positive mode, the analytes that reached the detector were ionized mainly by protonation [M + H]⁺ (such as amines, amino acids, lipids, aldehydes, ketones), and in negative mode due to the loss of a proton [M – H][−] (such as organic acids and sulfates) [36–39]. Non-polar organic molecules were not measured. The urban samples were coupled with the suburban samples according to the sampling date. The paired samples were analyzed in random order to avoid possible systematic errors. The instrument stability was monitored throughout the

analysis sequences by regularly injecting in-house prepared standard solutions (about 1 standard every 10 samples). Specifically, a 100 ppb caffeine solution was used for positive ion mode, and a 100 ppb phthalic acid solution was used for negative ion mode. The average deviation was <20% throughout the analytical run.

For the chromatographic separation, a C18 column (2.1 mm × 10 mm, 3 μm particle diameter, Fortis) was used. The binary pump system consisted of mobile phases A and B. Mobile phase A was ultrapure H₂O (18.2 MΩ/cm, PURELAB Option-S, Elga Labwater, Lane End, UK), and mobile phase B was ACN, both of which contained 0.1% *w/v* formic acid (Fisher Chemical LC/MS grade, Waltham, MA, USA). The flow rate was set to 300 μL/min, the column temperature to 30 °C, and the injection volume to 2 μL. A gradient elution program was run for 22 min, with the initial mobile phase B at 5% for 2 min, increasing linearly to 100% at 13 min, where it remained for an additional 2 min. Then, the mobile phase returned to its initial composition within a minute and remained as such for 6 min before the next injection.

The HPLC system was coupled with the mass spectrometer via a Heated Electro-Spray Ionization probe (HESI-II) that operated in both positive and negative ionization modes. Each sample was analyzed twice, in full MS positive mode (90–800 *m/z* range) and negative mode (117–800 *m/z*), thus the higher-energy collisional dissociation (HCD) cell was not used. The resolution was set to the highest setting (140,000 at 200 *m/z*), the AGC target (automatic gain control) was set to 3×10^6 for the c-trap, and the maximum IT (injection time) was 200 ms. For the source parameters, the spray voltage was set to +3.4 kV and −3.2 kV, respectively, the S-lens RF level (stacked-ring ion guide radio frequency) to 35 a.u., the sheath flow rate to 39 a.u. (arbitrary unit), the auxiliary gas flow rate to 16 a.u., the sweep gas flow rate to 0 a.u., the auxiliary gas heater temperature to 300 °C, and the capillary temperature to 300 °C. The instrument mass accuracy was externally calibrated prior to sample analysis with an in-house prepared STFA (sodium trifluoroacetate) solution [40]. The mass spectrometry .raw files were acquired in centroid mode.

To accumulate as much information as possible to compare the two sample groups, the Orbitrap mass spectrometer was operating in full MS mode for both positive and negative mode ESI ionization for a non-target analysis. High-resolution mass spectrometers offer selectivity, accurate mass measurements, and low limits of detection, making them ideal for non-target analysis [27].

2.4. Data Analysis

For the detection and integration of the chromatographic peaks/features, the open-source software Mzmine 4.0 was used [41]. A feature is a chromatographic peak, corresponding to a specific *m/z* and elution time. Noise levels of 5×10^4 and 1×10^4 were set for positive and negative ion modes, respectively. The rest of the feature recognition parameters were the Mzmine 4.0 default settings for HPLC-Orbitrap files (Table S1). Chromatographic peak area was used as a measure of intensity. Two lists of features were exported and further peak selection was done in an Excel spreadsheet environment. In particular, features that were present in both the blank and aerosol samples, i.e., the matrix background, were not investigated further if the average sample intensity was less than 5 times the average intensity of blank samples. Additionally, features detected in fewer than 25% of the samples were not investigated further. The Principal Component Analysis (PCA) and the volcano plots were generated using the online open-source software MetaboAnalyst 6.0 [42]. Missing values were replaced by one fifth of the minimum positive value of the respective feature intensity. The .raw files were visualized using Freestyle™ 1.5 (Thermo Scientific). The elemental composition of important features was calculated using Qual Browser (Thermo Xcalibur 4.2.47).

Only the elements C, H, O, N, S were considered for the elemental composition calculations. The N:C was restricted to between 0 and 1.3, with a maximum of 10 nitrogen atoms, the O:C to between 0 and 1.2, and the S:C to between 0 and 0.8, with a maximum

of 2 sulfur atoms [30,43]. The calculated Ring Double Bond Equivalent (RDBE) value for the neutral molecular formula was limited to integer numbers ranging from -1 to 20. The maximum error for features with $m/z > 130$ was set to ± 2.5 ppm. When multiple elemental composition candidates were calculated, the relative abundance of the isotopic pattern was the deciding factor. In positive mode, the ionization mechanism was assumed to be the protonation, with no fragmentation of the molecules and single charge. Regarding specific marker compounds, as our analysis was conducted in full MS mode, it was limited to elemental composition for each feature. Identifying chemical structures would require MS/MS spectra with multiple collision energy (CE) and library matching.

The Black Carbon (BC) concentration was continuously monitored in the urban station with an AE33 Aethalometer (Magee Scientific, Berkeley, CA, USA) [44]. The values were daily averaged and the Pearson correlation coefficient of BC with significant urban features in the positive mode was calculated in the Excel environment.

3. Results and Discussion

3.1. Features Detection and Total Intensity Comparison

The Mzmine analysis process resulted in the detection of 2809 and 3823 features for positive and negative modes, respectively. As a first step, the total intensity of every feature for all samples was summed for both modes. Samples from the urban station showed a higher total intensity compared to those from the suburban station. Specifically, compared to the suburban samples, the urban samples had on average a 55% higher total intensity in positive mode, and a 39% higher total intensity in negative mode (Figure 2). This is expected due to the intense anthropogenic activity in the urban environment, which leads to more particulate organic emissions. The higher percentage increase for the positive ion mode, compared to the negative ion mode, in the urban samples than in the suburban samples indicates that these wintertime anthropogenic emissions are richer in compounds that ionize better in positive mode rather than in negative mode.

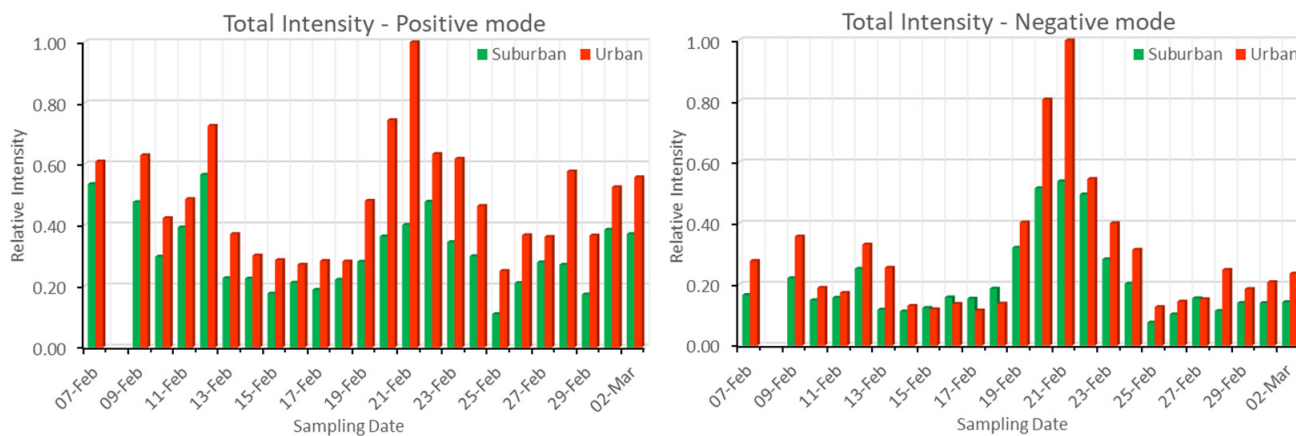


Figure 2. Total intensity for both modes and for the two stations. The relative intensity was set as 1 for the sample with the highest intensity.

It has to be noted that the mentioned total intensity does not represent the total organic molecules per sample. Ionization and transmission efficiencies for different compounds can vary significantly, making estimates based on peak areas among compounds prone to uncertainties [45].

For the urban samples, a significant correlation ($r = 0.86$, $n = 24$) was found between the two modes, whereas in suburban samples that was not the case ($r = 0.48$, $n = 24$) (Figure S1). This suggests that the urban environment may have more distinct sources of pollution, resulting in a more uniform chemical profile detectable in both modes than in the suburban samples. In the suburban area, the majority of air pollution is transported and therefore chemically transformed in the atmosphere. At the top of

this transported background atmospheric composition, which defines the baseline in Heraklion, pollutants from regional sources are added in the suburban station and further anthropogenic pollution is added in the city center. The long-range transported air masses have a larger variety of origins, as discussed in Section 2.1, and are the same for the two stations. This leads to a more diverse chemical profile at the urban station, with some compounds ionizing in only one mode.

On average, a 42% increase in the total PM₁₀ mass concentration (Figure S2) was measured gravimetrically for the urban environment, highlighting the significant impact of the local anthropogenic activities on total particulate matter concentrations. The urban environment had a PM₁₀ average concentration of 29 $\mu\text{g}/\text{m}^3$ and the suburban environment 20 $\mu\text{g}/\text{m}^3$, respectively. These results agree with those of Sohrab et al. [13], who reported higher urban than suburban PM₁₀ levels in Europe, especially during the residential heating periods.

3.2. Ion Detection Modes Comparison and Significant Feature Detection

To holistically compare the two ion modes, PCA was performed using the features after blank subtraction from the positive ion mode and the negative ion mode, separately.

PCA showed a clear separation between urban and suburban samples for positive ion mode features, unlike for negative ion mode ones (Figure 3). This is a first indication that positive mode ionization may be more suitable for this urban environment and sampling period for the detection of anthropogenic emission tracers.

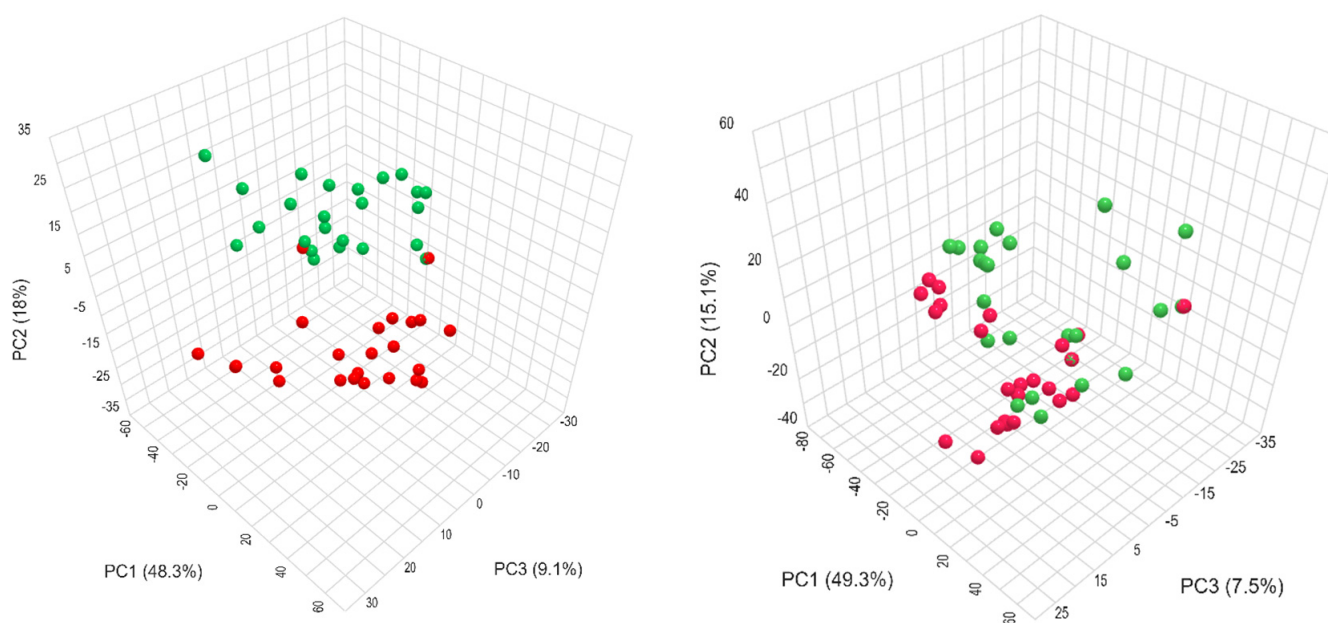


Figure 3. Results of 3d PCA for urban (red) and suburban samples (green) using positive ion mode features (left) and negative ion mode features (right). Log₁₀ data transformation was applied.

To further investigate the features responsible for this clustering, volcano plots were created for both ionization modes. Significant features for each station (Figure 4), in addition to the unique features, had at least a five times higher average concentration (fold change $\text{FC} > 5$) at that station than at the other station, and this difference is statistically significant by *t*-test with FDR (False Discovery Rate) corrected $p < 0.05$.

The results from the volcano plots also highlight the advantage of positive mode ionization relative to negative mode for detecting features from local urban emissions. Indeed, 20.5% of the features detected in the positive ion mode were classified as significant for the urban environment, compared to only 3.3% in the negative ion mode.

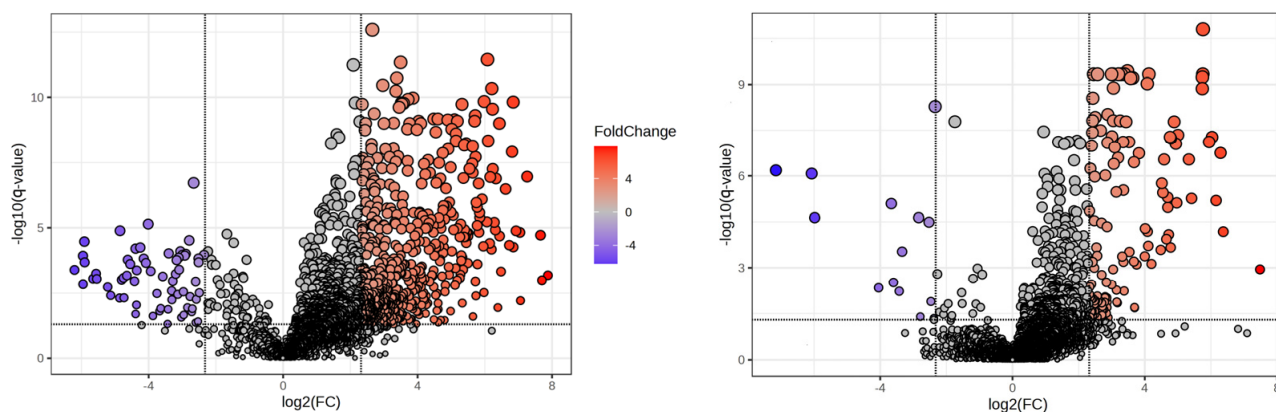


Figure 4. Comparison of volcano plots of urban and suburban samples for the positive ion mode (**left**) and the negative ion mode (**right**). The upper-right rectangular area in both plots highlights the significant urban features, and the upper-left area highlights the significant suburban features. FC = ratio of urban-to-suburban average intensities for each feature.

The number of significant suburban features is one order of magnitude lower than the significant urban features, for each ionization mode (Table 1). It should be noted that the suburban station is located in an area with agricultural activities, which could lead to the presence and therefore the detection of different organic compounds, compared to the urban environment where there are no such activities.

Table 1. Comparison of significant urban and suburban features by ionization mode.

Ionization Mode	Total Features	Urban Significant Features *	Suburban Significant Features *
Positive	2809	575 (20.5%)	65 (2.3%)
Negative	3823	128 (3.3%)	14 (0.4%)

* The percentages are relative to the total feature number for every mode at each location.

3.3. Significant Urban Features Related to Combustion Processes

During wintertime, the concentration levels of POA are expected to be higher compared to other seasons due to residential heating emissions. The average atmospheric BC concentration for the days studied was $1.5 \mu\text{g}/\text{m}^3$ (Figure S3). To narrow down the number of important features, the correlation coefficient (Pearson— r) between the daily averages of BC concentrations and the intensity values of each significant urban feature from the positive mode was calculated. Out of the 575 features, 409 features were found to have a correlation ($r > 0.6$) with BC. For these 409 features, the elemental composition was calculated (Table S2) to highlight the molecular fingerprint of these anthropogenic, possibly combustion-related, emissions that include the biomass burning and transport emissions. It should be noted that, in order to characterize a feature as a tracer for a pollution source with high confidence, more data points from observations over a longer time period and with higher temporal resolution are needed.

It is possible for a molecule to correspond to more than one feature due to multiple charging, adduct formation, and fragmentation. The features that were highly correlated ($r > 0.95$) and with a retention time difference of <0.025 min were clustered for further inspection. Out of the 409 significant urban features, 32 clusters were identified with the above-mentioned settings. In one of these clusters, one feature was classified as doubly charged $[\text{M} + 2\text{H}]^{2+}$, with the single-charged feature being on average 4.9 times more abundant.

The majority of these significant urban features have a measured m/z in the range of 200–260 m/z (Figure 5). Regarding the intensity-weighted number of C, C10 clearly

dominates the distribution. Molecules with a carbon number 20 or more have insignificant levels relative to the overall intensity.

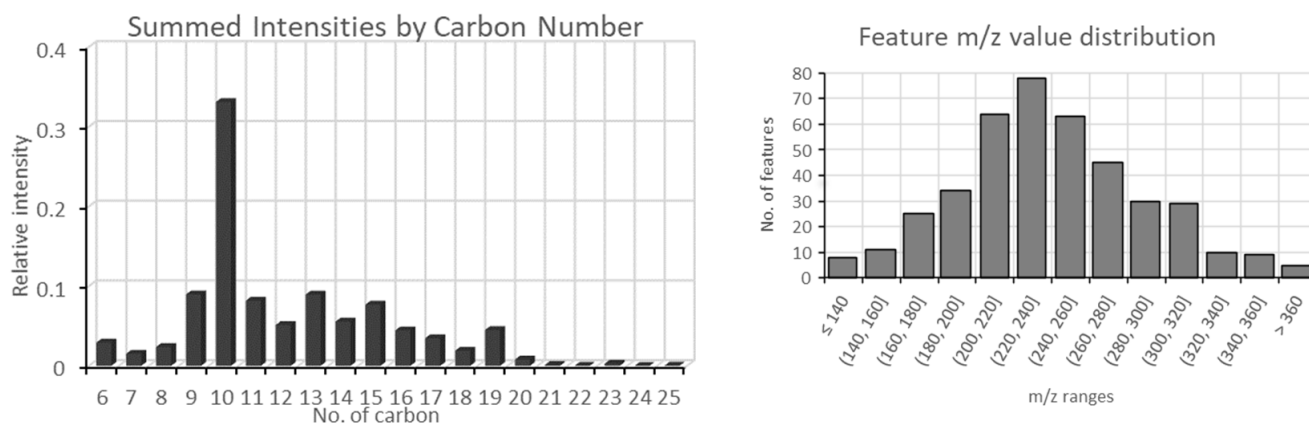


Figure 5. Combined abundance of the positive mode urban significant features related to combustion as a function of the number of carbon atoms (**left**). The m/z histogram for these features (**right**).

3.4. Elemental Composition Analysis of Significant Combustion-Related Urban Features

To further investigate the molecular fingerprint (Figure 6) of the positive mode significant features that correlate with combustion, the intensity-weighted average ratios of O:C and N:C ratios were calculated according to the following equations

$$\text{O:C} = \frac{\sum((\text{O:C})_i \times A_i)}{\sum A_i}$$

$$\text{N:C} = \frac{\sum((\text{N:C})_i \times A_i)}{\sum A_i}$$

with A_i being the average peak area for each feature i .

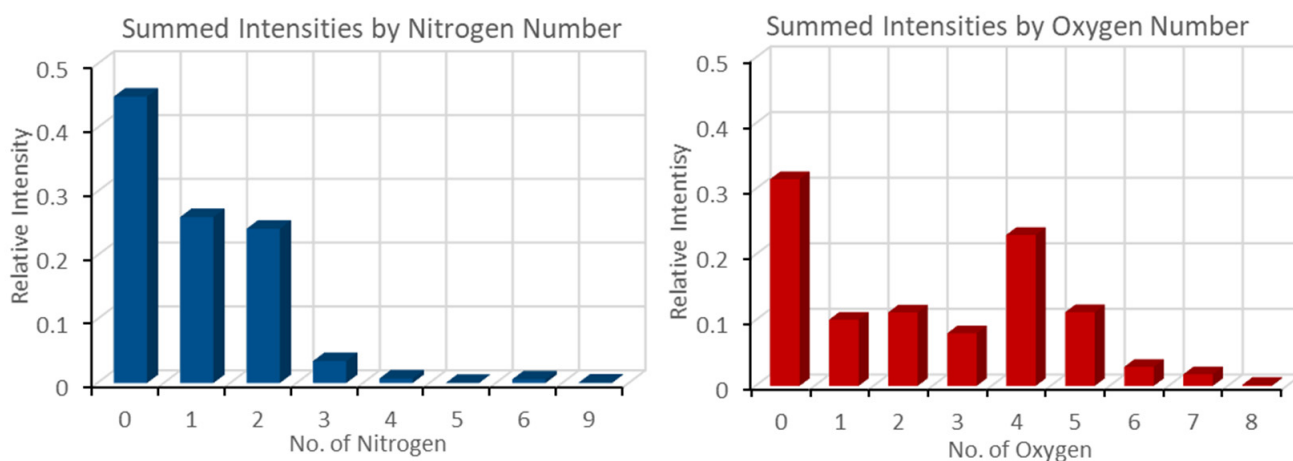


Figure 6. Combined abundance of the positive mode urban significant features related to combustion as a function of the number of nitrogen atoms (**left**) and oxygen atoms (**right**) in the calculated elemental composition of the respective feature.

Therefore, the O:C was estimated to be about 0.21 and the N:C about 0.09.

It should be noted that these values for O:C and N:C are typical for local combustion-related molecules. For instance, positive ion Orbitrap measurements in winter under high PM_{2.5} concentrations showed an O:C of 0.21 in Beijing, China, and of 0.27 in Mainz, Germany [46]. Gasoline car emissions have been reported to have an O:C = 0.04 and biomass burning OA an O:C = 0.31 [47]. In Zurich, the N:C ratio was determined to be 0.076 in winter and 0.029 in summer [30].

3.5. Volatility of Significant Combustion-Related Urban Features

The volatility of the atmospheric organic compounds is another important parameter that can characterize the pollution sources and chemistry processes such as aging [8]. Volatility of a compound can be quantified by the effective saturation mass concentration (C^*), which represents the concentration at which the compound exists in equal amounts in the gas and in the particulate phases during equilibrium [48], and equals the saturation mass concentration (C_0) when assuming ideal thermodynamic mixing [16].

The saturation mass concentration (C_0) was calculated for the significant combustion-related urban features according to the parameterizations of Li et al. [16], based on the calculated elemental composition (Table S2). According to the volatility value C_0 ($\mu\text{g}/\text{m}^3$), the organic molecules can be categorized as follows [6,49]:

1. Volatile Organic Compounds (VOC) ($C_0 > 3 \times 10^6$);
2. Intermediate Volatility Organic Compounds (IVOC) ($300 < C_0 < 3 \times 10^6$);
3. Semi-Volatile Organic Compounds (SVOC) ($0.3 < C_0 < 300$);
4. Low-Volatility Organic Compounds (LVOC) ($3 \times 10^{-4} < C_0 < 0.3$);
5. Extremely Low-Volatility Organic Compounds (ELVOC) ($C_0 < 3 \times 10^{-4}$).

The volatility class distribution of the organics present in the aerosol phase shows the abundance of the IVOC with a decreasing trend towards the ELVOC (Figure 7, left panel). This has also previously been reported for highly polluted urban environments [49]. OA undergo chemical transformations that affect their volatility. As the organic molecules age in the atmosphere, they typically become less volatile and more oxidized. This is also shown in Figure 7 (right panel) where the O:C ratio tends to anticorrelate with the volatility. Note that the presence of VOC species in the aerosol samples can be attributed to the adsorption of volatile molecules onto the quartz-fiber filters during sampling [50].

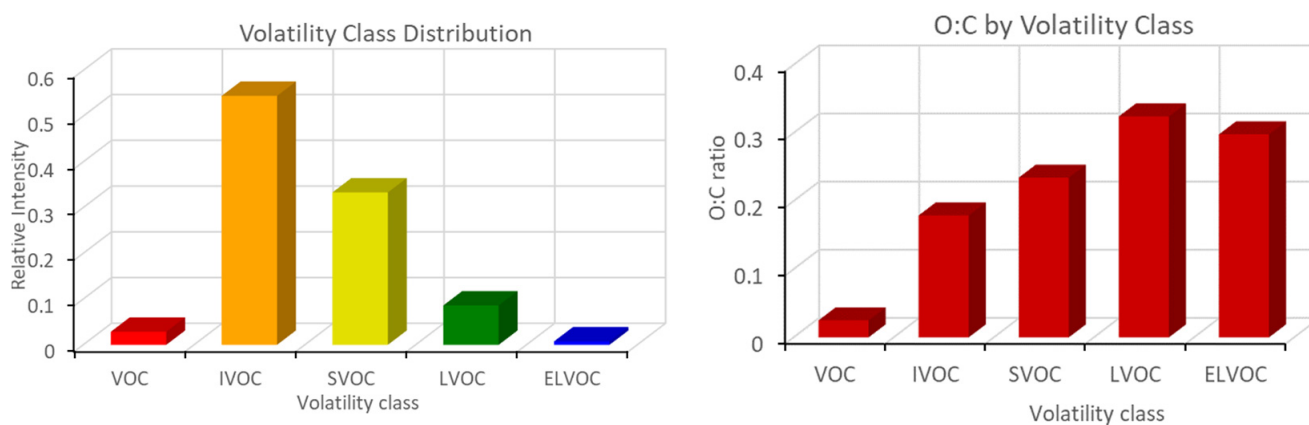


Figure 7. (left) Relative intensity of each volatility class, for the positive mode urban significant features related to combustion. (right) The estimated O:C ratio per volatility class from volatile (VOC) to extremely low volatility compounds (ELVOC).

To obtain a holistic estimation of the average volatility and to compare it with other studies, the intensity-weighted average $\log_{10}C_0$ was calculated for the highlighted organic matrix, resulting in a value of 2.46. It has been shown that there is a correlation between high concentrations of locally emitted urban PM_{2.5} and relatively high volatility. For Beijing, China, the $\log_{10}C_0$ was calculated to be 2.9 for high PM_{2.5} days and 1.6 for the low PM_{2.5} days. By comparison, Mainz, Germany, with the lowest PM_{2.5}, had a $\log_{10}C_0 = 0.9$ [49]. This indicates that the combustion-related significant urban molecules have, on average, a relatively high volatility as expected for fresh, low oxidized winter emissions.

4. Conclusions

This study used high-resolution Orbitrap mass spectrometry to analyze the PM10 organic aerosol composition in urban and suburban areas of Heraklion, Crete, Greece, aiming to investigate the molecular fingerprint of the local anthropogenic emissions during the winter pollution heating period in 2024. The results demonstrated that positive ionization mode was effective in detecting molecules related to local combustion processes, and 575 out of the total 2809 features were deemed significant. Urban samples exhibited higher total intensities in both positive and negative ion modes compared to suburban samples, indicating the influence of local anthropogenic activities. Also, significant correlation was observed between the majority of urban features and black carbon concentrations, underscoring the relevance of these features as potential tracers of combustion-related pollution. Combustion related features had an O:C of about 0.21 and an N:C about 0.09, similar to other studies. IVOC was found to be the major volatility class of organics in the urban aerosol with O:C of 0.18, while LVOC, with a relative intensity 6.6 times smaller, had the highest O:C ratio of about 0.32.

The findings emphasize the importance of advanced analytical techniques in understanding the complexities of urban air pollution. Analyzing samples from both urban and suburban stations helped to differentiate effectively the urban emissions from the long-range transported and background pollution. The elemental composition and volatility calculations of the significant urban features confirmed that the corresponding molecules are freshly emitted with low O:C ratios and relatively high volatility. Future research should expand on these findings across different seasons and locations to provide a more comprehensive understanding of urban air pollution characteristics. Also, efforts should be made to identify the associated molecules by conducting more detailed mass spectrometric measurements.

Supplementary Materials: The following supporting information can be downloaded at: <https://www.mdpi.com/article/10.3390/air2030018/s1>, Table S1. The processing wizard parameters of Mzmine, Figure S1. Scatter plots for the comparison of the polarity modes between urban and suburban stations in Heraklion, Crete, Greece, Figure S2. Daily average PM10 mass concentrations for the study period for the two stations in Heraklion, Crete, Greece, Figure S3. Daily average urban BC concentrations in Heraklion for the study period (left). Pearson r correlation values histogram for BC-significant positive mode urban features (right), Figure S4. Correlation of BC with urban total intensity of positive (left) and negative mode (right), Figure S5. Chromatographic peak of a significant urban feature (207.1589 m/z and RT 7.32 min) as an example. Lower panels show the corresponding full MS mass spectra at 7.31 min. Table S2. The calculated elemental composition for each significant combustion-related urban feature in positive ion mode.

Author Contributions: Conceptualization, E.S. and M.K.; methodology, E.S., A.C.C., S.A.P. and M.K.; data curation, E.S.; writing—original draft preparation, E.S.; writing—review and editing, E.S., A.C.C., S.A.P. and M.K.; visualization, E.S.; supervision, M.K.; funding acquisition, M.K. All authors have read and agreed to the published version of the manuscript.

Funding: This project has received funding from the European Union's Horizon 2020 research and innovation program under Ri-URBANS grant agreement No. 101036245 and Net4Cities grant number 101138405. It has also been supported by the Region of Crete and the University of Crete under the collaboration project SXEDIA.

Data Availability Statement: All relevant data have been included in this paper in the form of tables and figures. Specific data requests can be addressed by email to the corresponding authors.

Use of Artificial Intelligence: Artificial intelligence (AI) was used in the preparation of this manuscript for language editing and grammar.

Acknowledgments: We would like to express our sincere gratitude to Nikos Kalivitis and Aikaterini Faidra Kozonaki, members of the ECPL group, for their invaluable support and assistance regarding the measurements at the stations.

Conflicts of Interest: The authors declare no conflicts of interest. The funders had no role in the design of the study, in the collection, analyses, or interpretation of data, in the writing of the manuscript, or in the decision to publish the results.

Disclaimer: Where authors are identified as personnel of the International Agency for Research on Cancer/World Health Organization, the authors alone are responsible for the views expressed in this article and they do not necessarily represent the decisions, policies, or views of the International Agency for Research on Cancer/World Health Organization.

References

1. Zhang, R.; Wang, G.; Guo, S.; Zamora, M.L.; Ying, Q.; Lin, Y.; Wang, W.; Hu, M.; Wang, Y. Formation of Urban Fine Particulate Matter. *Chem. Rev.* **2015**, *115*, 3803–3855. [[CrossRef](#)] [[PubMed](#)]
2. Sofia, D.; Gioiella, F.; Lotrecchiano, N.; Giuliano, A. Mitigation Strategies for Reducing Air Pollution. *Environ. Sci. Pollut. Res.* **2020**, *27*, 19226–19235. [[CrossRef](#)] [[PubMed](#)]
3. Kanakidou, M.; Seinfeld, J.H.; Pandis, S.N.; Barnes, I.; Dentener, F.J.; Facchini, M.C.; Van Dingenen, R.; Ervens, B.; Nenes, A.; Nielsen, C.J.; et al. Organic Aerosol and Global Climate Modelling: A Review. *Atmos. Chem. Phys.* **2005**, *5*, 1053–1123. [[CrossRef](#)]
4. Chen, G.; Canonaco, F.; Tobler, A.; Aas, W.; Alastuey, A.; Allan, J.; Atabakhsh, S.; Aurela, M.; Baltensperger, U.; Bougiatioti, A.; et al. European Aerosol Phenomenology—8: Harmonised Source Apportionment of Organic Aerosol Using 22 Year-Long ACSM/AMS Datasets. *Environ. Int.* **2022**, *166*, 107325. [[CrossRef](#)]
5. Huang, R.J.; Zhang, Y.; Bozzetti, C.; Ho, K.F.; Cao, J.J.; Han, Y.; Daellenbach, K.R.; Slowik, J.G.; Platt, S.M.; Canonaco, F.; et al. High Secondary Aerosol Contribution to Particulate Pollution during Haze Events in China. *Nature* **2015**, *514*, 218–222. [[CrossRef](#)]
6. Murphy, B.N.; Donahue, N.M.; Robinson, A.L.; Pandis, S.N. A Naming Convention for Atmospheric Organic Aerosol. *Atmos. Chem. Phys.* **2014**, *14*, 5825–5839. [[CrossRef](#)]
7. Li, H.Z.; Dallmann, T.R.; Li, X.; Gu, P.; Presto, A.A. Urban Organic Aerosol Exposure: Spatial Variations in Composition and Source Impacts. *Environ. Sci. Technol.* **2018**, *52*, 415–426. [[CrossRef](#)]
8. Jimenez, J.L.; Canagaratna, M.R.; Donahue, N.M.; Prevot, A.S.H.; Zhang, Q.; Kroll, J.H.; DeCarlo, P.F.; Allan, J.D.; Coe, H.; Ng, N.L.; et al. Evolution of Organic Aerosols in the Atmosphere. *Science* **2009**, *326*, 1525–1529. [[CrossRef](#)] [[PubMed](#)]
9. Koulouri, E.; Saarikoski, S.; Theodosi, C.; Markaki, Z.; Gerasopoulos, E.; Kouvarakis, G.; Mäkelä, T.; Hillamo, R.; Mihalopoulos, N. Chemical Composition and Sources of Fine and Coarse Aerosol Particles in the Eastern Mediterranean. *Atmos. Environ.* **2008**, *42*, 6542–6550. [[CrossRef](#)]
10. Chen, G.; Canonaco, F.; Slowik, J.; Daellenbach, K.; Tobler, A.; Petit, J.-E.; Favez, O.; Stavroulas, I.; Mihalopoulos, N.; Gerasopoulos, E.; et al. Real-Time Source Apportionment of Organic Aerosols in Three European Cities. *Environ. Sci. Technol.* **2022**, *2022*, 15290–15297. [[CrossRef](#)]
11. Bougiatioti, A.; Zampas, P.; Koulouri, E.; Antoniou, M.; Theodosi, C.; Kouvarakis, G.; Saarikoski, S.; Mäkelä, T.; Hillamo, R.; Mihalopoulos, N. Organic, Elemental and Water-Soluble Organic Carbon in Size Segregated Aerosols, in the Marine Boundary Layer of the Eastern Mediterranean. *Atmos. Environ.* **2013**, *64*, 251–262. [[CrossRef](#)]
12. Stavroulas, I.; Bougiatioti, A.; Grivas, G.; Paraskevopoulou, D.; Tsagkaraki, M.; Zampas, P.; Liakakou, E.; Gerasopoulos, E.; Mihalopoulos, N. Sources and Processes That Control the Submicron Organic Aerosol Composition in an Urban Mediterranean Environment (Athens): A High Temporal-Resolution Chemical Composition Measurement Study. *Atmos. Chem. Phys.* **2019**, *19*, 901–919. [[CrossRef](#)]
13. Sohrab, S.; Csikos, N.; Szilassi, P. Effects of Land Use Patterns on PM10 Concentrations in Urban and Suburban Areas. A European Scale Analysis. *Atmos. Pollut. Res.* **2023**, *14*, 101942. [[CrossRef](#)]
14. Heikkinen, L.; Äijälä, M.; Daellenbach, K.R.; Chen, G.; Garmash, O.; Aliaga, D.; Graeffe, F.; Rätty, M.; Luoma, K.; Aalto, P.; et al. Eight Years of Sub-Micrometre Organic Aerosol Composition Data from the Boreal Forest Characterized Using a Machine-Learning Approach. *Atmos. Chem. Phys.* **2021**, *21*, 10081–10109. [[CrossRef](#)]
15. Robinson, A.L.; Donahue, N.M.; Shrivastava, M.K.; Weitkamp, E.A.; Sage, A.M.; Grieshop, A.P.; Lane, T.E.; Pierce, J.R.; Pandis, S.N. Rethinking Organic Aerosols: Semivolatile Emissions and Photochemical Aging. *Science* **2007**, *315*, 1259–1262. [[CrossRef](#)]
16. Li, Y.; Pöschl, U.; Shiraiwa, M. Molecular Corridors and Parameterizations of Volatility in the Chemical Evolution of Organic Aerosols. *Atmos. Chem. Phys.* **2016**, *16*, 3327–3344. [[CrossRef](#)]
17. Li, M.; Yu, S.; Chen, X.; Li, Z.; Zhang, Y.; Song, Z.; Liu, W.; Li, P.; Zhang, X.; Zhang, M.; et al. Impacts of Condensable Particulate Matter on Atmospheric Organic Aerosols and Fine Particulate Matter (PM2.5) in China. *Atmos. Chem. Phys.* **2022**, *22*, 11845–11866. [[CrossRef](#)]
18. Simoneit, B.R.T.; Elias, V.O.; Kobayashi, M.; Kawamura, K.; Rushdi, A.I.; Medeiros, P.M.; Rogge, W.F.; Didyk, B.M. Sugars—Dominant Water-Soluble Organic Compounds in Soils and Characterization as Tracers in Atmospheric Particulate Matter. *Environ. Sci. Technol.* **2004**, *38*, 5939–5949. [[CrossRef](#)]
19. Hu, Q.H.; Xie, Z.Q.; Wang, X.M.; Kang, H.; Zhang, P. Levoglucosan Indicates High Levels of Biomass Burning Aerosols over Oceans from the Arctic to Antarctic. *Sci. Rep.* **2013**, *3*. [[CrossRef](#)]
20. Theodosi, C.; Panagiotopoulos, C.; Nouara, A.; Zampas, P.; Nicolaou, P.; Violaki, K.; Kanakidou, M.; Sempéré, R.; Mihalopoulos, N. Sugars in Atmospheric Aerosols over the Eastern Mediterranean. *Prog. Oceanogr.* **2018**, *163*, 70–81. [[CrossRef](#)]

21. Gogou, A.; Stratigakis, N.; Kanakidou, M.; Stephanou, E.G. Organic Aerosols in Eastern Mediterranean: Components Source Reconciliation by Using Molecular Markers and Atmospheric Back Trajectories. *Org. Geochem.* **1996**, *25*, 79–96. [[CrossRef](#)]
22. Pedrosa-Pamies, R.; Parinos, C.; Sanchez-Vidal, A.; Calafat, A.; Canals, M.; Velaoras, D.; Mihalopoulos, N.; Kanakidou, M.; Lampadariou, N.; Gogou, A. Atmospheric and Oceanographic Forcing Impact Particle Flux Composition and Carbon Sequestration in the Eastern Mediterranean Sea: A Three-Year Time-Series Study in the Deep Ierapetra Basin. *Front. Earth Sci.* **2021**, *9*, 591948. [[CrossRef](#)]
23. Magda, C.; Bim, G.; Gyorgy, V.; Wu, W.; Reinhilde, V.; Vlada, P.; Jan, C.; Pascal, G.; Meinrat, O.A.; Paulo, A.; et al. Formation of Secondary Organic Aerosols Through Photooxidation of Isoprene. *Science* **2004**, *303*, 1173–1176. [[CrossRef](#)]
24. Kavouras, I.G.; Michalopoulos, N.; Stephanou, E.G. Formation of Atmospheric Particles from Organic Acids Produced by Forests. *Nature* **1998**, *395*, 683–686. [[CrossRef](#)]
25. Zhang, Q.; Jimenez, J.L.; Canagaratna, M.R.; Ulbrich, I.M.; Ng, N.L.; Worsnop, D.R.; Sun, Y. Understanding Atmospheric Organic Aerosols via Factor Analysis of Aerosol Mass Spectrometry: A Review. *Anal. Bioanal. Chem.* **2011**, *401*, 3045–3067. [[CrossRef](#)]
26. Eliuk, S.; Makarov, A. Evolution of Orbitrap Mass Spectrometry Instrumentation. *Annu. Rev. Anal. Chem.* **2015**, *8*, 61–80. [[CrossRef](#)] [[PubMed](#)]
27. He, X.; Huang, X.H.; Ma, Y.; Huang, C.; Yu, J.Z. Unambiguous Analysis and Systematic Mapping of Oxygenated Aromatic Compounds in Atmospheric Aerosols Using Ultrahigh-Resolution Mass Spectrometry. *Anal. Chem.* **2024**, *96*, 1880–1889. [[CrossRef](#)]
28. Hollender, J.; Schymanski, E.L.; Singer, H.P.; Ferguson, P.L. Nontarget Screening with High Resolution Mass Spectrometry in the Environment: Ready to Go? *Environ. Sci. Technol.* **2017**, *51*, 11505–11512. [[CrossRef](#)]
29. Pereira, K.L.; Ward, M.W.; Wilkinson, J.L.; Sallach, J.B.; Bryant, D.J.; Dixon, W.J.; Hamilton, J.F.; Lewis, A.C. An Automated Methodology for Non-Targeted Compositional Analysis of Small Molecules in High Complexity Environmental Matrices Using Coupled Ultra Performance Liquid Chromatography Orbitrap Mass Spectrometry. *Environ. Sci. Technol.* **2021**, *55*, 7365–7375. [[CrossRef](#)]
30. Daellenbach, K.; Kourtev, I.; Vogel, A.; Bruns, E.; Jiang, J.; Petäjä, T.; Jaffrezo, J.L.L.; Aksoyoglu, S.; Kalberer, M.; Baltensperger, U.; et al. Impact of Anthropogenic and Biogenic Sources on the Seasonal Variation in the Molecular Composition of Urban Organic Aerosols: A Field and Laboratory Study Using Ultra-High-Resolution Mass Spectrometry. *Atmos. Chem. Phys.* **2019**, *19*, 5973–5991. [[CrossRef](#)]
31. Zittis, G.; Almazroui, M.; Alpert, P.; Ciais, P.; Cramer, W.; Dahdal, Y.; Fnais, M.; Francis, D.; Hadjinicolaou, P.; Howari, F.; et al. Climate Change and Weather Extremes in the Eastern Mediterranean and Middle East. *Rev. Geophys.* **2022**, *60*, e2021RG000762. [[CrossRef](#)]
32. Urdiales-Flores, D.; Zittis, G.; Hadjinicolaou, P.; Osipov, S.; Klingmüller, K.; Mihalopoulos, N.; Kanakidou, M.; Economou, T.; Lelieveld, J. Drivers of Accelerated Warming in Mediterranean Climate-Type Regions. *NPJ Clim. Atmos. Sci.* **2023**, *6*, 97. [[CrossRef](#)]
33. Lelieveld, J.; Berresheim, H.; Borrmann, S.; Crutzen, P.J.; Dentener, F.J.; Fischer, H.; Feichter, J.; Flatau, P.J.; Heland, J.; Holzinger, R.; et al. Global Air Pollution Crossroads over the Mediterranean. *Science* **2002**, *298*, 794–799. [[CrossRef](#)] [[PubMed](#)]
34. Mihalopoulos, N.; Stephanou, E.; Kanakidou, M.; Pilitsidis, S.; Bousquet, P. Tropospheric Aerosol Ionic Composition in the Eastern Mediterranean Region. *Tellus B Chem. Phys. Meteorol.* **1997**, *49*, 314–326. [[CrossRef](#)]
35. Stein, A.F.; Draxler, R.R.; Rolph, G.D.; Stunder, B.J.B.; Cohen, M.D.; Ngan, F. NOAA's Hysplit Atmospheric Transport and Dispersion Modeling System. *Bull. Am. Meteorol. Soc.* **2015**, *96*, 2059–2077. [[CrossRef](#)]
36. Banerjee, S.; Mazumdar, S. Electrospray Ionization Mass Spectrometry: A Technique to Access the Information beyond the Molecular Weight of the Analyte. *Int. J. Anal. Chem.* **2012**, *2012*, 282574. [[CrossRef](#)] [[PubMed](#)]
37. Oss, M.; Krueve, A.; Herodes, K.; Leito, I. Electrospray Ionization Efficiency Scale of Organic Compound. *Anal. Chem.* **2010**, *82*, 2865–2872. [[CrossRef](#)]
38. Mayhew, A.W.; Topping, D.O.; Hamilton, J.F. New Approach Combining Molecular Fingerprints and Machine Learning to Estimate Relative Ionization Efficiency in Electrospray Ionization. *ACS Omega* **2020**, *5*, 9510–9516. [[CrossRef](#)]
39. Leito, I.; Herodes, K.; Huopolainen, M.; Virro, K.; Künnapas, A.; Krueve, A.; Tanner, R. Towards the Electrospray Ionization Mass Spectrometry Ionization Efficiency Scale of Organic Compounds. *Rapid Commun. Mass Spectrom.* **2008**, *22*, 379–384. [[CrossRef](#)]
40. Moini, M.; Jones, B.L.; Rogers, R.M.; Jiang, L. Sodium Trifluoroacetate as a Tune/Calibration Compound for Positive- and Negative-Ion Electrospray Ionization Mass Spectrometry in the Mass Range of 100–4000 Da. *Am. Soc. Mass Spectrom.* **1998**, *9*, 977–980. [[CrossRef](#)]
41. Pluskal, T.; Castillo, S.; Villar-Briones, A.; Orešič, M. MZmine 2: Modular Framework for Processing, Visualizing, and Analyzing Mass Spectrometry-Based Molecular Profile Data. *BMC Bioinform.* **2010**, *11*, 395. [[CrossRef](#)]
42. Xia, J.; Wishart, D.S. Web-Based Inference of Biological Patterns, Functions and Pathways from Metabolomic Data Using MetaboAnalyst. *Nat. Protoc.* **2011**, *6*, 743–760. [[CrossRef](#)]
43. Kind, T.; Fiehn, O. Seven Golden Rules for Heuristic Filtering of Molecular Formulas Obtained by Accurate Mass Spectrometry. *BMC Bioinform.* **2007**, *8*, 105. [[CrossRef](#)] [[PubMed](#)]
44. Drinovec, L.; Močnik, G.; Zotter, P.; Prévôt, A.S.H.; Ruckstuhl, C.; Coz, E.; Rupakheti, M.; Sciare, J.; Müller, T.; Wiedensohler, A.; et al. The “Dual-Spot” Aethalometer: An Improved Measurement of Aerosol Black Carbon with Real-Time Loading Compensation. *Atmos. Meas. Tech.* **2015**, *8*, 1965–1979. [[CrossRef](#)]

45. Wang, K.; Huang, R.J.; Brüggemann, M.; Zhang, Y.; Yang, L.; Ni, H.; Guo, J.; Wang, M.; Han, J.; Bilde, M.; et al. Urban Organic Aerosol Composition in Eastern China Differs from North to South: Molecular Insight from a Liquid Chromatography-Mass Spectrometry (Orbitrap) Study. *Atmos. Chem. Phys.* **2021**, *21*, 9089–9104. [[CrossRef](#)]
46. Wang, K.; Zhang, Y.; Huang, R.J.; Cao, J.; Hoffmann, T. UHPLC-Orbitrap Mass Spectrometric Characterization of Organic Aerosol from a Central European City (Mainz, Germany) and a Chinese Megacity (Beijing). *Atmos. Environ.* **2018**, *189*, 22–29. [[CrossRef](#)]
47. Aiken, A.C.; Decarlo, P.F.; Kroll, J.H.; Worsnop, D.R.; Huffman, J.A.; Docherty, K.S.; Ulbrich, I.M.; Mohr, C.; Kimmel, J.R.; Sueper, D.; et al. O/C and OM/OC Ratios of Primary, Secondary, and Ambient Organic Aerosols with High-Resolution Time-of-Flight Aerosol Mass Spectrometry. *Environ. Sci. Technol.* **2008**, *42*, 4478–4485. [[CrossRef](#)] [[PubMed](#)]
48. Donahue, N.M.; Robinson, A.L.; Stanier, C.O.; Pandis, S.N. Coupled Partitioning, Dilution, and Chemical Aging of Semi volatile Organics. *Environ. Sci. Technol.* **2006**, *40*, 2635–2643. [[CrossRef](#)] [[PubMed](#)]
49. Wang, K.; Zhang, Y.; Tong, H.; Han, J.; Fu, P.; Huang, R.J.; Zhang, H.; Hoffmann, T. Molecular-Level Insights into the Relationship between Volatility of Organic Aerosol Constituents and PM_{2.5} Air Pollution Levels: A Study with Ultrahigh-Resolution Mass Spectrometry. *Environ. Sci. Technol.* **2024**, *58*, 7947–7957. [[CrossRef](#)] [[PubMed](#)]
50. Kristensen, K.; Bilde, M.; Aalto, P.P.; Petäjä, T.; Glasius, M. Denuder/Filter Sampling of Organic Acids and Organosulfates at Urban and Boreal Forest Sites: Gas/Particle Distribution and Possible Sampling Artifacts. *Atmos. Environ.* **2016**, *130*, 36–53. [[CrossRef](#)]

Disclaimer/Publisher’s Note: The statements, opinions and data contained in all publications are solely those of the individual author(s) and contributor(s) and not of MDPI and/or the editor(s). MDPI and/or the editor(s) disclaim responsibility for any injury to people or property resulting from any ideas, methods, instructions or products referred to in the content.